The Journal of Chemical Physics

Computation of solid–fluid interfacial free energy in molecular systems using thermodynamic integration

Cite as: J. Chem. Phys. **153**, 154504 (2020); https://doi.org/10.1063/5.0028653
Submitted: 06 September 2020 . Accepted: 25 September 2020 . Published Online: 15 October 2020

Ravi Kumar Reddy Addula, and Sudeep N. Punnathanam

The Journal of Chemical Physics ARTICLE scitation.org/journal/jcp

Computation of solid–fluid interfacial free energy in molecular systems using thermodynamic integration

Cite as: J. Chem. Phys. 153, 154504 (2020); doi: 10.1063/5.0028653
Submitted: 6 September 2020 • Accepted: 25 September 2020 •
Published Online: 15 October 2020

Ravi Kumar Reddy Addula and Sudeep N. Punnathanam[a)]

AFFILIATIONS

Department of Chemical Engineering, Indian Institute of Science, Bangalore 560012, India

[a)]Author to whom correspondence should be addressed: sudeep@iisc.ac.in

ABSTRACT

In this article, we present two methods based on thermodynamic integration for computing solid–fluid interfacial free energy for a molecular system. As a representative system, we choose two crystal polymorphs of orcinol (5-methylbenzene-1,3-diol) as the solid phase and chloroform and nitromethane as the liquid phase. The computed values of the interfacial free energy are then used in combination with the classical nucleation theory to predict solvent induced polymorph selectivity during crystallization of orcinol from solution.

I. INTRODUCTION

Free energies of interfaces formed between fluid and solid phases play an important role in many natural and industrial processes such as wetting and spreading of coatings on solid surface,[1] enhanced oil recovery from reservoirs,[2] role of surfactants in detergents, development of self-cleaning surfaces (super hydrophobic surfaces),[3] crystal nucleation,[4] and crystal growth.[5] However, the accurate measurement of solid–fluid interfacial free energy from experiments is still a challenging task. Some of the methods developed over the years for measuring interfacial free energy from experiments include estimation from experimental nucleation rates[4] and from contact angle measurements.[6] Estimates from these methods, however, suffer from large errors[7] and are unable to obtain crystal facet specific interfacial free energy.[4,5,7] The precise values of these estimates are essential to understand and control the aforesaid processes. Hence, it is imperative to develop methods for computation of interfacial free energies using molecular simulations.

The most widely used strategy to compute solid–fluid interfacial free energy relies on thermodynamic integration. The literature on this subject is vast, and we only discuss a few of them that are directly relevant to the study presented in this article. One of the common approaches is to reversibly cleave the solid and liquid phases and then bring them together to create the solid–fluid interface. We use the term "cleaving wall" to describe these classes of methods. One of the earliest studies using this method was conducted by Broughton and Gilmer[8] who computed the interfacial free energy between crystal and its melt made up of Lennard-Jones particles. A similar strategy was used by Davidchack and Laird[9] to compute melt-crystal interfacial free energy for hard sphere systems. Both the studies suffered from problems of hysteresis in the thermodynamic integration when the cleaving walls were removed. These were caused by changes in the location of the interface due to simultaneous melting and freezing of the two interfaces present in the system. Benjamin and Horbach[10] addressed this problem by introducing extremely short-ranged and impenetrable Gaussian flat walls to confine the liquid and crystal phases. Qi, Zhou, and Fichthorn[11] developed a multi-scheme thermodynamic integration method that is inspired by the "cleaving-wall" method of Benjamin and Horbach[10] to compute the interfacial free energy of the Ag–ethylene glycol interface. The method can be implemented using open-source molecular dynamics packages such as Large-scale Atomic/Molecular Massively Parallel Simulator (LAMMPS).[12] Even though this method has potential applicability for a wide range of systems, it is necessary to devise specific strategies to account for the periodic boundary conditions (PBC) in the solid and liquid phases along the thermodynamic integration path. In addition to the cleaving wall method, there have been other methods developed to compute either the interfacial free energy or the contact angles of liquid drops on surfaces. These include the interface fluctuation method,[13]

phantom wall method,[14] mold-integration method,[15] calculation of spreading coefficient using transition matrix Monte Carlo,[16] and direct estimation of contact angles.[17]

In this article, we present two new and independent methods based on thermodynamic integration to compute solid–fluid interfacial free energy. In their present formulation, these methods work only when (i) the solid and liquid phases are mutually immiscible and (ii) there is no surface diffusion of molecules in the solid phase. In both these methods, we use a recently developed method of Reddy A and Punnathanam[18] to incorporate the free energy contributions of the solid phase into the estimation of the interfacial free energy. The first method is a variant of the cleaving wall method as discussed above. The second method is called the "adsorption method" in which the free energy of the liquid phase is computed by integrating an adsorption isotherm. We apply these methods to compute the interfacial free energy between different crystal planes of orcinol (5-methylbenzene-1,3-diol) and two different solvents, chloroform and nitromethane. The motivations for choosing this system are twofold. First, we consider this to be a representative molecular system that contains most of the complexities one may encounter while computing solid–liquid interfacial free energy. Second, orcinol exists in many crystal polymorphs, and in this study, we consider two anhydrous polymorphs called form I and form II.[19] In experiments, form I is formed when chloroform is used as a solvent and form II is obtained when nitromethane is used as a solvent. If the selectivity is determined by the rates of crystal nucleation of each polymorph, then the knowledge of the solid–fluid interfacial free energy would enable us to predict solvent-induced polymorph selectivity using the classical nucleation theory. All the simulations presented in this paper have been performed using the LAMMPS[12] molecular dynamics package. The input files required to perform these simulations are available in the supplementary material.

II. CLEAVING WALL METHOD

Consider an interface between a pure solid phase comprising molecules of component A and a pure liquid phase comprising molecules of component B. The Gibbs free energy, G, of this two phase system can be written as

$$G = \mu_A N_A + \mu_B N_B + \gamma A,$$

where μ_i and N_i are the chemical potential and the number of molecules of component i respectively, γ is the interfacial free-energy, and A is the interfacial area. Since the solid and liquid phases are pure systems, we have

$$G^{(s)} = \mu_A N_A,$$
$$G^{(l)} = \mu_B N_B,$$

where $G^{(s)}$ and $G^{(l)}$ are the Gibbs free energies of the bulk solid and liquid phases consisting of N_A and N_B molecules, respectively, at the same temperature and pressure. Hence, the interfacial free energy can be expressed as

$$\gamma = \frac{G - G^{(l)} - G^{(s)}}{A}. \quad (1)$$

In this method, we compute free energy of a solid slab in contact with the liquid and then use Eq. (1) to compute the interfacial free energy. The free-energy of the two phase system has a $\ln V$ term that arises from the translation of the center of mass of the solid slab (see the Appendix for explanation). Obviously, the value of γ should not depend on the volume, V, of the system. To avoid spurious contributions from this translational degree of freedom, the center of mass of the solid phase is kept fixed. Accordingly,

$$\gamma = \frac{G^* - G^{(l)} - G^{*(s)}}{A}, \quad (2)$$

where the asterisk indicates that the center of mass of the solid phase is fixed.

The interfacial free energy using Eq. (2) is computed from a series of simulations in the NPT ensemble. During the simulations, only the length of the simulation box perpendicular to the solid–fluid interface is varied, and the interfacial area is constant. The isothermal–isobaric partition function for this two phase system with the fixed center of mass for the solid phase is given by

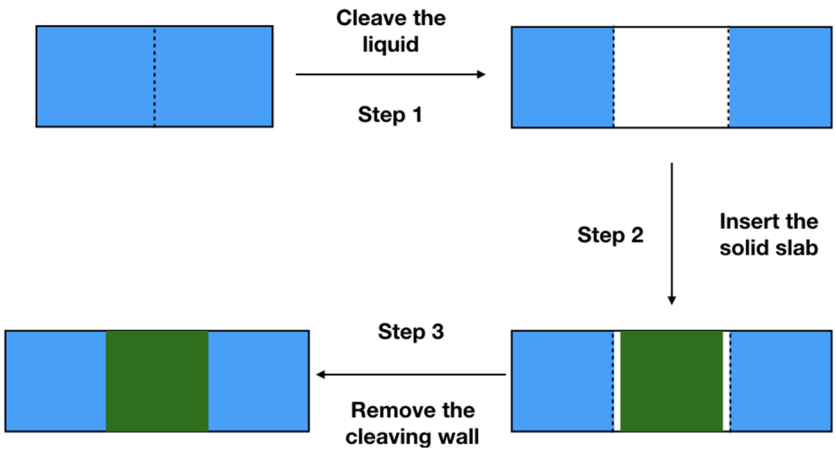

FIG. 1. Step-wise illustration of the cleaving wall method. Blue indicates the liquid phase, and green indicates the solid phase.

$$\Delta(N_A, N_B, P, T) = C_A^* C_B \int e^{-\beta(U_A+U_B+U_{AB})} \times e^{-\beta PV} d\mathbf{r}^{N_A+N_B-1} dV, \quad (3)$$

where C_A^* and C_B are constants comprising integrals over the momenta and the permutation of molecules for the solid and liquid phases, respectively. The numerical values of these constants do not contribute to the interfacial free energy. The terms U_A and U_B represent intermolecular interactions within the solid and liquid phases, while U_{AB} represent interactions between the solid and liquid phases. The notation $\mathbf{r}^{N_A+N_B-1}$ indicates that the positions of all atoms are sampled in such a way that the center of mass of the solid phase is fixed. The RHS of Eq. (3) is evaluated by thermodynamic integration from a homogeneous liquid phase as follows:

Step 1: The initial state consists of a homogeneous liquid composed of N_B molecules of solvent B at pressure P and temperature T. In step 1, the liquid is cleaved by introducing an external potential, U_W. This creates space for inserting the solid slab. The free energy change in this step is denoted as ΔG_1.

Step 2: A solid slab of N_A molecules of solute A is inserted into the space created inside the liquid in step 1. The center of mass of the solid is kept fixed during this insertion. The free energy change in this step is denoted as ΔG_2.

Step 3: The external potential, U_W, is removed from the system resulting in a solid slab surrounded by the liquid phase. The free energy change in this step is denoted as ΔG_3.

A schematic representation of the steps involved is shown in Fig. 1. Mathematically, the evaluation of the RHS of Eq. (3) is expressed as follows:

$$\begin{aligned}\Delta(N_A, N_B, P, T) &= C_B \int e^{-\beta U_B} e^{-\beta PV} d\mathbf{r}^{N_B} dV \times \frac{\int e^{-\beta(U_W+U_B)} e^{-\beta PV} d\mathbf{r}^{N_B} dV}{\int e^{-\beta U_B} e^{-\beta PV} d\mathbf{r}^{N_B} dV} \\ &\times C_A^* \int e^{-\beta U_A} d\mathbf{r}^{N_A-1} \times \frac{\int e^{-\beta(U_{AB}+U_A+U_B+U_W)} e^{-\beta PV} d\mathbf{r}^{N_A+N_B-1} dV}{\int e^{-\beta(U_A+U_B+U_W)} e^{-\beta PV} d\mathbf{r}^{N_A+N_B-1} dV} \\ &\times \frac{\int e^{-\beta(U_A+U_B+U_{AB})} e^{-\beta PV} d\mathbf{r}^{N_A+N_B-1} dV}{\int e^{-\beta(U_W+U_A+U_B+U_{AB})} e^{-\beta PV} d\mathbf{r}^{N_A+N_B-1} dV} \\ &= \Delta_B(N_B, P, T) e^{-\beta\Delta G_1} Q_A^{*(\text{slab})}(N_A, T) e^{-\beta\Delta G_2} e^{-\beta\Delta G_3}, \end{aligned} \quad (4)$$

where the superscript (slab) represents a solid slab made of N_A molecules exposed to vacuum. Substituting Eq. (4) into Eq. (2), we get

$$\begin{aligned}\gamma &= \frac{\Delta G_1 + \Delta G_2 + \Delta G_3 + F_A^{*(\text{slab})} - G^{*(\text{s})}}{A} \\ &= \frac{\Delta G_1 + \Delta G_2 + \Delta G_3 + (F_A^{*(\text{slab})} - F_A^{*(\text{s})}) - PV^{(\text{s})}}{A}, \end{aligned} \quad (5)$$

where F is the Helmholtz free energy and $V^{(\text{s})}$ is the volume of the bulk solid phase containing N_A molecules at pressure P and temperature T. The various terms in the RHS of Eq. (5) are evaluated as follows.

A. Calculation of ΔG_1 and ΔG_3

Since the LAMMPS[12] molecular dynamics package was used in performing all the simulations, the following form of the wall potential, U_W, was used. The wall potential is created by inserting N_W atoms, arranged in a rectangular lattice, in a plane perpendicular to the direction in which the liquid is to be cleaved. These wall atoms are kept fixed at their initial positions and only interact with the fluid molecules as follows:

$$U_W = \sum_{i=1}^{N_W} \sum_{j=1}^{N_B} A \exp\left(\frac{\lambda - r_{ij}}{B}\right) - C \exp\left(\frac{\lambda - r_{ij}}{D}\right), \quad (6)$$

where r_{ij} is the distance between the ith wall atom and one atom of the jth fluid molecule and A, B, C, D, and λ are parameters of the potential. The two terms in the wall potential represent repulsive and attractive interactions with the fluid molecules. The repulsive term is responsible for cleaving the liquid phase. The role of the attractive term is explained in the next step. Each lattice point in the rectangular lattice contains both attractive and repulsive sites. The introduction of the wall is done in two steps: (i) insertion with a small value of $\lambda = \lambda_{\min}$ and (ii) increase in the value of λ from $\lambda_{\min}$ to $\lambda_{\max}$. The change in the free energy due to the introduction of the wall is computed via thermodynamic integration as follows:

$$\begin{aligned}\Delta G_1 &= -k_B T \ln\left[\frac{\int e^{-\beta(U_W(\lambda_{\min})+U_B)} e^{-\beta PV} d\mathbf{r}^{N_B} dV}{\int e^{-\beta U_B} e^{-\beta PV} d\mathbf{r}^{N_B} dV}\right] \\ &\quad - k_B T \ln\left[\frac{\int e^{-\beta(U_W(\lambda_{\max})+U_B)} e^{-\beta PV} d\mathbf{r}^{N_B} dV}{\int e^{-\beta(U_W(\lambda_{\min})+U_B)} e^{-\beta PV} d\mathbf{r}^{N_B} dV}\right] \\ &= -k_B T \ln\left\langle e^{-\beta U_W(\lambda_{\min})} \right\rangle + \int_{\lambda_{\min}}^{\lambda_{\max}} \left\langle \frac{\partial U_W}{\partial \lambda} \right\rangle d\lambda. \end{aligned} \quad (7)$$

A similar procedure is used to compute ΔG_3 as follows:

$$\begin{aligned}\Delta G_3 &= k_B T \ln\left[\frac{\int e^{-\beta(U_W(\lambda_{\max})+U_A+U_B+U_{AB})} e^{-\beta PV} d\mathbf{r}^{N_A+N_B-1} dV}{\int e^{-\beta(U_W(\lambda_{\min})+U_A+U_B+U_{AB})} e^{-\beta PV} d\mathbf{r}^{N_A+N_B-1} dV}\right] \\ &\quad + k_B T \ln\left[\frac{\int e^{-\beta(U_W(\lambda_{\min})+U_A+U_B+U_{AB})} e^{-\beta PV} d\mathbf{r}^{N_A+N_B-1} dV}{\int e^{-\beta(U_A+U_B+U_{AB})} e^{-\beta PV} d\mathbf{r}^{N_A+N_B-1} dV}\right] \\ &= -\int_{\lambda_{\min}}^{\lambda_{\max}} \left\langle \frac{\partial U_W}{\partial \lambda} \right\rangle d\lambda + k_B T \ln\left\langle e^{-\beta U_W(\lambda_{\min})} \right\rangle. \end{aligned} \quad (8)$$

B. Calculation of ΔG_2

ΔG_2 is the free energy due to interactions between the solid and liquid phases and is computed as follows:

$$\Delta G_2 = -k_B T \ln\left[\frac{\int e^{-\beta(U_{AB}+U_A+U_B+U_W)} e^{-\beta PV} d\mathbf{r}^{N_A+N_B-1} dV}{\int e^{-\beta(U_A+U_B+U_W)} e^{-\beta PV} d\mathbf{r}^{N_A+N_B-1} dV}\right] = -k_B T \ln\left\langle e^{-\beta U_{AB}}\right\rangle. \quad (9)$$

The importance of the attractive term in the wall potential U_W in the evaluation of ΔG_2 can be explained as follows. While using Eq. (9) to compute ΔG_2, it is important that the structure of the surrounding fluid phase undergoes minimal perturbation when the U_{AB} interactions are turned on. At temperatures much lower than the critical point of the liquid, the saturated pressure is very low. In such a scenario, a purely repulsive wall can lead to the occurrence of a drying transition near the liquid–wall interface.[20] If the solid slab is introduced within the cleaved region, the attractive interactions between the fluid and the solid can cause a sharp increase in the liquid density near the interface. Hence, the role of the attractive term is to prevent the occurrence of drying transition near the wall fluid interface while the fluid is being cleaved using the wall potential.

C. Calculation of $F_A^{*(\text{slab})}$ and $F_A^{*(\text{s})}$

The solid state free energies, $F_A^{*(\text{slab})}$ and $F_A^{*(\text{s})}$, are computed using thermodynamic integration from a reference state. The reference state for both these calculations is a non-interacting Einstein crystal with the fixed center of mass. In a non-interacting Einstein crystal, there are no intermolecular interactions present and all the atoms are attached to their respective lattice point via a harmonic spring. The thermodynamic integration is performed in two steps. In the first step, the intermolecular interactions between the molecules are turned on resulting in an interacting Einstein crystal. In the second step, the Einstein field is turned off resulting in the system of interest. If we denote U_{ec} as the Einstein-field, then

$$F_A^* = -k_B T \ln C_A^* \int e^{-\beta\left(U_{\text{ec}}+U_A^{\text{intra}}\right)} d\mathbf{r}^{N_A-1} - k_B T \ln\left[\frac{\int e^{-\beta(U_{\text{ec}}+U_A)} d\mathbf{r}^{N_A-1}}{\int e^{-\beta\left(U_{\text{ec}}+U_A^{\text{intra}}\right)} d\mathbf{r}^{N_A-1}}\right] - k_B T \ln\left[\frac{\int e^{-\beta U_A} d\mathbf{r}^{N_A-1}}{\int e^{-\beta(U_{\text{ec}}+U_A)} d\mathbf{r}^{N_A-1}}\right] \quad (10)$$

$$= F_{\text{ec}}^* + \Delta F_1 + \Delta F_2, \quad (11)$$

where U_A^{intra} is the energy due to intramolecular interaction of the molecules. Since the reference state is a non-interacting Einstein crystal containing N_A molecules, it is the same for both the slab and the bulk solid. Hence, the difference $F_A^{*(\text{slab})} - F_A^{*(\text{s})}$ can be computed as

$$F_A^{*(\text{slab})} - F_A^{*(\text{s})} = \left(\Delta F_1^{(\text{slab})} + \Delta F_2^{(\text{slab})}\right) - \left(\Delta F_1^{(\text{s})} + \Delta F_2^{(\text{s})}\right). \quad (12)$$

The methods for computing ΔF_1 and ΔF_2 are similar to the ones described by Reddy A and Punnathanam.[18]

III. ADSORPTION METHOD

In this method, the interfacial free energy is determined by computing the Helmholtz free energy, F, of the two phase system, which can be expressed as

$$F(N_A, N_B, V, T) = -PV + \mu_A N_A + \mu_B N_B + \gamma A. \quad (13)$$

If we choose a dividing surface such that the surface excess for component A vanishes, i.e., $N_A^{(\text{s})} = N_A$, then

$$F = F_A^{(\text{s})} + F_B^{(\text{l})} + \mu_B N_B^{(\sigma)} + \gamma A, \quad (14)$$

where the superscript (σ) denotes the surface excess. Similar to the previous method, we omit the free energy contributions due to the three translational degrees of freedom to avoid spurious contributions to the γ. To implement this criterion, we used the concept of the Einstein molecule[18,21,22] and keep the position of one atom of one of the molecules fixed. In addition, we also have the equation, $F_B^{(\text{l})} = -PV^{(\text{l})} + \mu_B N_B^{(\text{l})}$. Hence, the interfacial free energy can be computed as

$$\gamma = \frac{F^* - F_A^{*(\text{s})} + PV^{(\text{l})} - \mu_B N_B}{A}. \quad (15)$$

The calculation of F^* in this method starts from a crystalline solid slab consisting of N_A molecules of component A exposed to vacuum followed by the addition of N_B molecules of component B in the surrounding space. Figure 2 depicts the central idea behind the adsorption method. The detailed steps involved in this computation are as follows:

- Step 1: We start from a non-interacting Einstein molecule slab containing N_A molecules of component A exposed to vacuum. The strength of the harmonic spring is equal to Λ_0. The Helmholtz free energy for this reference state is denoted by F_0^*.
- Step 2: The intermolecular interactions, U_A, are turned on to create an interacting Einstein molecule slab. The free energy change, $\Delta F_1^{(\text{slab})}$, in this step is computed via thermodynamic perturbation.
- Step 3: The strength of the harmonic spring in the Einstein-field is reduced to Λ_1. The reason for not reducing this value to zero is explained in the next step. The free energy change, $\Delta F_2^{(\text{slab})}$, in this step is computed via thermodynamic integration.
- Step 4: In this step, N_B molecules of component B are added to the vacuum surrounding the solid slab. However, in the systems being studied here, the temperature is below the critical temperature of the component B. As a result, the fluid will undergo a vapor-to-liquid phase transition during the addition of the molecules. To avoid this scenario, the fluid is made supercritical by reducing the well-depth of the Lennard-Jones interaction between the molecules. For the purpose of improved clarity while discussing this step, we shall denote the molecules with the reduced interaction as C. The free energy change in this step is computed by integrating the adsorption isotherm that gives the change in the grand potential. The grand potential, Ω, is a Legendre transform of the Helmholtz free energy, F,

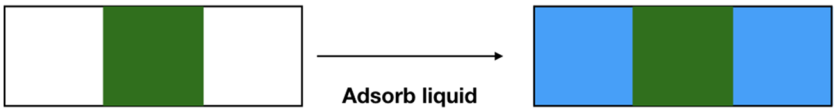

FIG. 2. Illustration of the central idea of computing interfacial free energy using the adsorption method. Blue indicates the liquid phase, and green indicates the solid phase.

and is defined for this two-component system as $\Omega = F - \mu_C N_B$. The change in the free energy of this step is given by

$$\Delta\Omega = -\int_{-\infty}^{\mu_C} N d\mu_C'. \tag{16}$$

In order to compute free energy change using the above equation, a series of simulations are performed in the canonical ensemble with the number of molecules of component C varying from 0 to N_B. The chemical potential of B is determined from the Gibbs–Duhem equation for pure systems at constant temperature, i.e., $d\mu_C = v_C dP$, where v_C is the volume per molecule of component C at pressure P. Substituting into Eq. (16), we get

$$\Delta\Omega = -\int_0^{P_C} N v_C dP = -\int_0^{\rho_C} N v_C \left(\frac{\partial P}{\partial \rho}\right) d\rho. \tag{17}$$

During the simulations, we measure the density of the fluid far away from the interface. The value of the pressure at a given density is obtained from simulations of the bulk fluid at constant temperature. The upper limit, P_C, in the above integral is the pressure at which N_B molecules are present in the system. Since the fluid is supercritical, the pressure of the liquid at the highest density, P_C, is very high. Such a high pressure can and almost always destroy the crystalline structure of the solid slab. To avoid this scenario, the molecules of the solid are still attached to their lattice sites by the harmonic spring with value Λ_1 for the spring constant. The overall change in the Helmholtz free energy, ΔF_3, during this step can be expressed as

$$\Delta F_3 = \Delta\Omega + \mu_C N_B. \tag{18}$$

Step 5: In this step, the Lennard-Jones interaction between the fluid molecules is increased to its full strength and the electrostatic interactions are also turned on. The free energy change, ΔF_4, during this step is computed via thermodynamic integration.

Step 6: In the previous step, when the full attractive interactions between the fluid molecules are turned on, the pressure of the fluid is reduced considerably and is nearly equal to the desired value. It is now safe to turn off the Einstein-field interactions in the solid slab. Hence, in this final step, the value of the spring constant of the Einstein field is reduced from Λ_1 to zero. The change in the free energy, ΔF_5, is computed via thermodynamic integration.

The overall free energy of the two-phase system can be expressed as

$$F^* = F_0^* + \Delta F_1^{(\text{slab})} + \Delta F_2^{(\text{slab})} + \Delta\Omega + \Delta F_4 + \Delta F_5 + \mu_C N_B. \tag{19}$$

The free energy of the bulk solid is computed similarly,[18] i.e.,

$$F^{*(\text{s})} = F_0^* + \Delta F_1^{(\text{s})} + \Delta F_2^{(\text{s})}. \tag{20}$$

The difference in the chemical potentials $\mu_C - \mu_B$ is computed as follows:

$$\mu_C(P_C) - \mu_B(P) = \left[\mu_C(P_C) - \mu_C(P_C')\right] + \left[\mu_C(P_C') - \mu_B(P)\right]$$
$$= -\int_{P_C'}^{P_C} v_C dP + \left[\mu_C(P_C') - \mu_B(P)\right] \tag{21}$$

$$= \Delta\mu_1 + \Delta\mu_2, \tag{22}$$

where P_C' is the pressure at which the density of C is equal to the density of B at pressure P. The term within the square brackets in the RHS of the above equation is computed via thermodynamic integration by turning on the Lennard-Jones interaction from the reduced strength to full strength. The value of the interfacial free energy is computed from Eq. (15) and Eqs. (19)–(22). It is important to note that the cross-sectional area A should be multiplied by a factor of 2 to account for the two surfaces created in both cleaving wall and adsorption methods.

IV. VALIDATION OF CLEAVING WALL METHOD WITH A LENNARD-JONES SYSTEM

The accuracy of the proposed methods is tested on a system comprising Lennard-Jones particles. The system is similar to the one

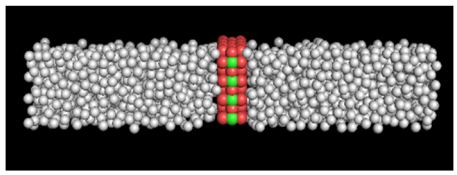

FIG. 3. Snapshot of the Lennard-Jones solid in contact with the Lennard-Jones liquid. The solid particles are shown in red, and the liquid particles are shown in gray. The particles forming the cleaving wall are shown in green.

TABLE I. Potential parameters for the wall potential in Eq. (6) for the Lennard-Jones system.

	$\frac{A}{\epsilon_{ff}}$	$\frac{B}{\sigma_{ff}}$	$\frac{C}{\epsilon_{ff}}$	$\frac{D}{\sigma_{ff}}$
Liquid	3.3333	0.2857	3.50	0.3714
Vapor	3.3333	0.2857	2.50	0.3714

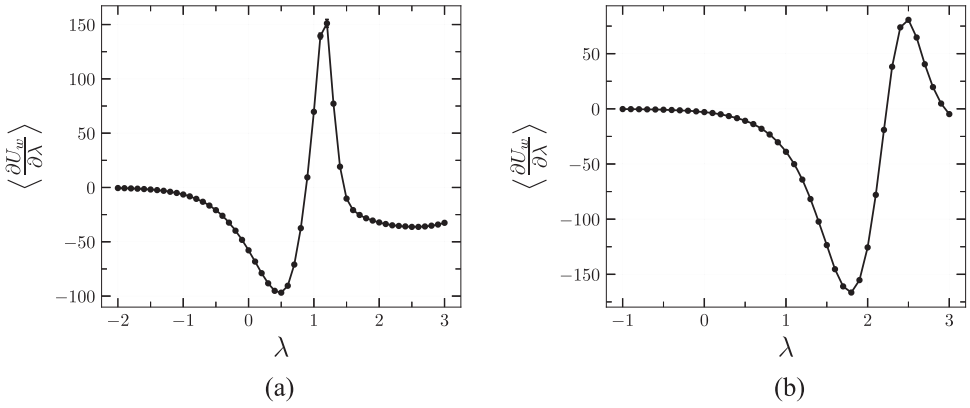

FIG. 4. Variation of the integrand during computation of (a) ΔG_1 and (b) ΔG_3 for the Lennard-Jones system. The size of the error bars corresponds to a confidence interval of 95%.

TABLE II. Change in the free energy per unit cross-sectional area for the various steps of the cleaving wall method applied to the Lennard-Jones system. The asterisk indicates that the values are in reduced units. The figure in the parentheses is the uncertainty in the last digit for a confidence interval of 95%.

	Liquid				Vapor			$\cos\theta$
ΔG_1^*	ΔG_2^*	ΔG_3^*	γ_{sl}^*	ΔG_1^*	ΔG_2^*	ΔG_3^*	γ_{sv}^*	
−0.824(4)	−0.065(1)	0.980(3)	0.091(5)	0.071(1)	−0.001(1)	−0.050(1)	0.020(1)	−0.30(2)

studied by Grzelak and Errington[16] where the solid–vapor–liquid contact angle, θ, was computed using Young's equation,

$$\cos\theta = \frac{\gamma_{sv} - \gamma_{sl}}{\gamma_{lv}}, \tag{23}$$

where γ_{sl}, γ_{sv}, and γ_{lv} are the solid–liquid, solid–vapor, and liquid–vapor interfacial free energies, respectively. The solid consists of three layers of a face-centered cubic crystal with the 100 plane exposed to the fluid. The fluid particles interact with $\epsilon_{ff} = 1.0$ and $\sigma_{ff} = 1.0$. The Lennard-Jones parameters for the solid–fluid interaction are $\epsilon_{sf} = 0.5$ and $\sigma_{sf} = 1.1$. The solid atoms are kept frozen at their lattice positions. The Lennard-Jones interaction is truncated and shifted at a cutoff distance $r_{ij}^c = 2.5\sigma_{ij}$. The system is studied at a reduced temperature $k_BT/\epsilon_{ff} = 0.9$ and at the coexistence pressure $P\sigma_{ff}^3/\epsilon_{ff} = 0.031\,467$.

A snapshot of the solid in contact with the liquid phase is shown in Fig. 3. The solid consists of 96 particles, and the cross-sectional area is $7.57\sigma_{ff} \times 7.57\sigma_{ff}$. The liquid phase contains 1500 particles, and the vapor phase contains 100 particles. The cleaving wall is constructed from a total of 16 sites[23] arranged in a square lattice and located in the x–y plane at the center of the simulation box. The potential parameters for the wall potential in Eq. (6) are given in Table I. The values of $\lambda_{\min}$ for computing ΔG_1 andΔG_3 are $-2\sigma_{ff}$ and $-\sigma_{ff}$, respectively. The upper limit $\lambda_{\max} = 3\sigma_{ff}$. The numerical integrations for computing ΔG_1 and ΔG_3 are performed using the trapezoidal rule with a spacing of $0.1\sigma_{ff}$ in the values of λ. Each simulation was run for a period of 2 000 000 steps during the equilibration stage and 5 000 000 steps during the production stage with the time step for integration set to 0.001. The temperature was controlled using the Nose–Hoover thermostat.[24] The variation of the integrands in computation of ΔG_1 and ΔG_3 are shown in Fig. 4. The results from the simulations on this system are given in Table II. Since $F_A^{*(\text{slab})}$ is the same for both liquid and vapor, it is not computed. The value of γ_{lv} is taken from Ref. 16 and set to 0.235. The contact angle as computed from Young's equation is $\cos\theta = -0.30(2)$, which is in close agreement with the value of $\cos\theta = -0.33(3)$ reported in Ref. 16.

V. SOLID–LIQUID INTERFACIAL FREE ENERGY FOR A MOLECULAR SYSTEM

In this section, we present the results of computation of solid–liquid interfacial free energy between orcinol and the two solvents, chloroform and nitromethane (see Fig. 5). Orcinol and nitromethane are modeled using the Optimized Potentials for Liquid Simulations-All Atom (OPLS-AA) forcefield, while chloroform is modeled using the OPLS-UA (United Atom) forcefield (4-site

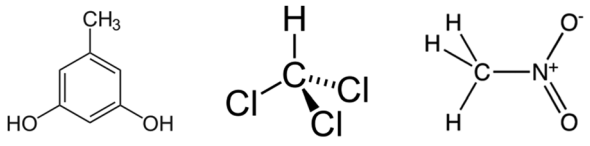

FIG. 5. Structural formula of (a) orcinol, (b) chloroform, and (c) nitromethane.

TABLE III. Area of the solid–fluid interface for different crystal planes of the orcinol polymorphs.

Plane	Form I (Å^2)	Form I (Å^2)
100	40.72 × 37.76	50.20 × 48.66
010	40.72 × 37.76	55.14 × 48.66
001	40.72 × 40.72	55.14 × 50.20

model).[25,26] The Lennard-Jones interactions were truncated and shifted at 12 Å, and the electrostatic interactions were computed using Particle–Particle–Particle–Mesh (PPPM).[27] The study was conducted at a temperature of 215 K and a pressure of 1 atm. Under these conditions, the solubilities of orcinol polymorphs are very low and there is also no surface diffusion of the orcinol molecules. The structure of the crystal polymorphs was obtained from the Cambridge Structural Database, and the interfacial free energy is computed for the 100 plane for both the crystal polymorphs. Initially, NPT simulations were performed to determine the density of the bulk solid phase under the above conditions. From these simulations, the lattice constants were determined to be a = 20.36 Å, b = 20.36 Å, and c = 6.29 Å for form I and a = 13.78 Å, b = 16.73 Å, and c = 24.33 Å for form II.

A. Cleaving wall method

The molecular dynamics simulations for computing the terms ΔG_i consisted of an equilibration stage of 1 ns and a production stage of 1 ns, while those for computing the terms ΔF_i consisted of an equilibration stage of 2 ns and a production stage of 5 ns.

The solid slab of form I polymorph consisted of 384 molecules, and that of form II polymorph consisted of 768 molecules. The dimensions of the interfacial area are given in Table III. The numbers of molecules of solvent were 1500 and 2000 for systems containing polymorphs form I and form II, respectively. The values of the spring constants, Λ_0, in the Einstein field for computing the solid state free energies were 20 000 (kcal/mol)/Å^2 for hydrogen atoms and 5000 (kcal/mol)/Å^2 for the rest. For simulations that contained the harmonic spring, the temperature was controlled using the Bussi thermostat,[28] while those without the harmonic springs used the Nose–Hoover thermostat.[24] The values of the wall potential parameters in Eq. (6) were A = 1.0 kcal/mol, B = 1.0 Å, C = 1.05 kcal/mol, and D = 1.4 Å for all the solvent and polymorph combinations studied in this work. The lower (λ_{min}) and upper limits (λ_{max}) of the integral for computing ΔG_1 were −4 Å and 34 Å, respectively. The lower limit (λ_{min}) of integral for computing ΔG_3 was 12 Å and 20 Å, respectively, when we study the polymorphs of form I and form II. A typical variation of the integrands in Eqs. (7) and (8) is shown in Fig. 6.

The numerical integration was carried out using the trapezoidal rule. For computing ΔG_2, we generated 200 configurations for the solid slab and for each of these configurations, and the averages were computed over a molecular dynamics trajectory of 1 ns. Since the simulations were performed using LAMMPS, currently, it is not possible to keep only the center of mass of the solid (and not the liquid) phase fixed in an NPT simulation. Instead, the center of mass of the solid is tethered to its initial position via a harmonic spring with a strength of 10 000 (kcal/mol)/Å^2. During the simulations, the fluctuation in the center of mass position was in the order of 10^{-5} Å, which is very small. Hence, we assume that the averages computed in these simulations have negligible errors. This assumption was validated *post priori* when the computed values of γ matched those obtained from the adsorption method.

B. Adsorption method

The duration of all the molecular dynamics simulations consisted of an equilibration run of 2 ns and a production run of 5 ns. The number of molecules and dimensions of the solid phase are the same as those used in the cleaving wall method. The length of the simulation box perpendicular to the interface was determined from an *NPT* simulation of the two-phase system at T = 215 K and P = 1 atm while keeping the interfacial area constant. The numbers of chloroform molecules were 1500 and 2000, and the lengths of the simulation box were 162.08 Å and 156.10 Å when the solid slab was form I and form II, respectively. In the case of nitromethane, the numbers of molecules were 2222 and 2960, and the box lengths were 162.08 Å and 156.10 Å for form I and form II, respectively. The value of the spring constants in the Einstein field at the reduced strength is Λ_1 = 100 kcal/mol. Similar to the cleaving wall method, the simulations that contained the harmonic spring used the Bussi thermostat,[28] while those without the harmonic springs used the Nose–Hoover

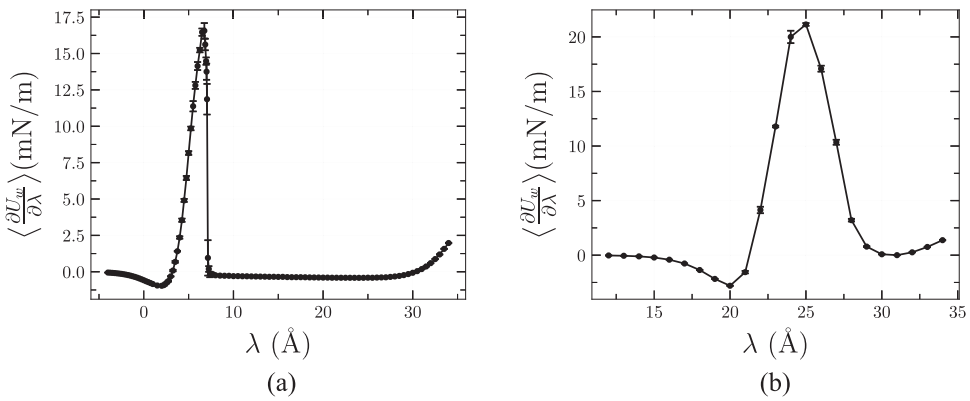

FIG. 6. Variation of the integrand during computation of (a) ΔG_1 and (b) ΔG_3 for the 100 plane of form I polymorph with chloroform. The size of the error bars corresponds to a confidence interval of 95%.

TABLE IV. Numerical values of the coefficients of Eq. (24).

	Chloroform	Nitromethane
B_2	−0.7662	−0.4135
B_3	1.3388	1.884
B_4	−0.6865	0.2545
B_5	0.0070	−1.0871
B_6	0.8569	3.36

thermostat.[24] To keep the chloroform and nitromethane supercritical during step 3, the value of ϵ in the Lennard-Jones interaction was reduced by a factor of 3.5 and partial charges on all the atoms were set to zero. For performing the integration using Eq. (17), one has to know the pressure of the fluid as a function of the bulk density, i.e., an equation of state for the fluid. This was determined by performing a series of NPT simulations of the bulk fluid at $T = 215$ K. The data from the simulations were fitted to the following equation of state:

$$Z = \frac{PV}{Nk_BT} = 1 + B_2\rho + B_3\rho^2 + B_4\rho^3 + B_5\rho^4 + B_6\rho^5, \qquad (24)$$

where the unit of ρ is g/cc. The numerical values of the coefficients for chloroform and nitromethane are given in Table IV. The variation of integrand in Eq. (17) with density is shown in Fig. 7 for the case where the 100 plane of form I is exposed to chloroform. $\Delta\Omega$ is computed by first fitting the integrand to a polynomial of degree four in density and then integrating the fitted polynomial.

C. Results

The computed values of the various terms needed for estimating the interfacial free energy using the cleaving wall method are given in Table V, and those using the adsorption method are given in Table VI. As we can see, the values of the interfacial free energy from the two methods are in agreement with each other. Since the same value of the free energy is obtained from completely different paths, we can confidently claim that the values computed are not only thermodynamically consistent but also accurate.

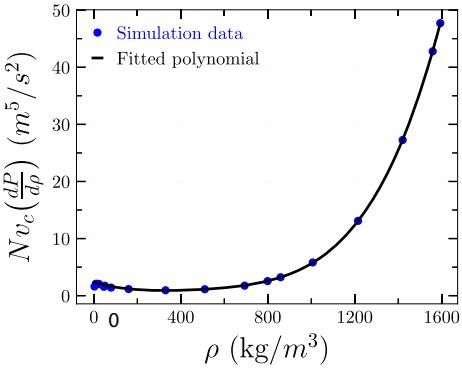

FIG. 7. Variation of the integrand in Eq. (17) with pressure of the fluid. The interface is the 100 plane of form I, and the fluid is chloroform. The fitted curve is a fourth degree polynomial. The size of the error bars corresponds to a confidence interval of 95%.

VI. SOLVENT INDUCED CRYSTAL POLYMORPHISM IN ORCINOL

The experiments performed by Mukherjee *et al.*[19] have shown that form I of orcinol is obtained when chloroform is used as a solvent and form II is obtained when the solvent is nitromethane. The common hypothesis for this solvent induced polymorphism is that the polymorph with the highest rate of nucleation is the one that will form upon crystallization from a solution. The rate of nucleation is exponentially dependent on the free energy of formation of the critical nucleus, and according to the Classical Nucleation Theory (CNT), this free energy, ΔG^*, is given as

TABLE V. Change in the free energy per unit cross-sectional area for the various steps of the cleaving wall method while computing interfacial free energy of the orcinol–solvent interface. The figure in the parentheses is the uncertainty in the last digit for a confidence interval of 95%. All the values have units of mN/m.

	Chloroform		Nitromethane	
	Form I	Form II	Form I	Form II
ΔG_1	25.7(3)	25.7(3)	35.1(6)	35.1(6)
ΔG_2	−0.011(2)	−7.0(3)	−0.16(1)	−4.9(3)
ΔG_3	−80.8(8)	−68.5(4)	−96(1)	−86(1)
$\Delta F_1^{(\mathrm{slab})}$	−1527.9(3)	−1807.4(5)	−1527.9(3)	−1807.4(5)
$\Delta F_2^{(\mathrm{slab})}$	−5527.5(6)	−6013.1(3)	−5527.5(6)	−6013.1(3)
$\Delta F_1^{(\mathrm{s})}$	−1647.6(1)	−1938.6(4)	−1647.6(1)	−1938.6(4)
$\Delta F_2^{(\mathrm{s})}$	−5527.3(2)	−5995.9(3)	−5527.3(2)	−5995.9(3)
$PV^{(\mathrm{s})}$	0.206	0.279	0.206	0.279
γ	64(1)	64(1)	59(1)	58(1)

TABLE VI. Change in the free energy per unit cross-sectional area for the various steps of the adsorption method while computing interfacial free energy of the orcinol–solvent interface. The figure in the parentheses is the uncertainty in the last digit for a confidence interval of 95%. All the values have units of mN/m.

	Chloroform		Nitromethane	
	Form I	Form II	Form I	Form II
$\Delta F_1^{(\mathrm{slab})}$	−1527.9(3)	−1810.2(3)	−1527.9(3)	−1810.2(3)
$\Delta F_2^{(\mathrm{slab})}$	−3694.2(2)	−4251.8(2)	−3694.2(2)	−4251.8(2)
$\Delta\Omega$	−1360(1)	−1177(1)	−2292(2)	−2000(1)
ΔF_4	−1647(1)	−1389(1)	−7234(1)	−6075(1)
ΔF_5	−1844.9(3)	−1777.8(6)	−1840(1)	−1778(1)
$\Delta\mu_1$	40(2)	115.5(8)	−17(2)	60.3(5)
$\Delta\mu_2$	2922.7(3)	2417.5(3)	9492(1)	7979(1)
$\Delta F_1^{(\mathrm{s})}$	−1647.7(2)	−1938.6(4)	−1647.7(2)	−1938.6(4)
$\Delta F_2^{(\mathrm{s})}$	−5529.5(3)	−5997.3(4)	−5529.5(3)	−5997.3(4)
$PV^{(\mathrm{l})}$	0.62	0.52	0.62	0.52
γ	65(3)	63(2)	63(3)	60(2)

$$\Delta G^* = \frac{16\pi\gamma^3}{3|\rho^{(\mathrm{s})}\Delta\mu|^2}, \tag{25}$$

where $\rho^{(\mathrm{s})}$ is the density of the solid phase and $\Delta\mu$ is the difference in the chemical potential of the solute in the solid phase and in solution. If this expression describes the nucleation process, then the polymorph with a lower value of γ should be the one favored to nucleate from a given solution. Strictly speaking, γ for a growing crystal is an orientationally averaged quantity, and the crystal facet with the lowest γ contributes the most. Computing the interfacial free energy for all possible combinations of facets and solvents is very expensive. Instead, we computed the interfacial free energy for a select few facets, namely, the 100, 010, and 001 planes, in contact with both the solvents. Of the two methods described above, the adsorption method was more cumbersome to implement. Hence, we used the cleaving wall method to compute the interfacial free energies for the different crystal planes. The results from our calculations are given in Tables VII and VIII. From Table VII, we observe that the interfacial free energy of form I polymorph with chloroform is higher than that of form II. Hence, CNT predicts that the polymorph form II will nucleate from a solution of orcinol in chloroform, a result that is at variance with the experimental observation. It might be possible that there might be other crystal planes of form I that have lower interfacial free energy. In the case of crystallization from nitromethane solution, the values of γ are lower for form II, which should lead to its crystallization instead of form I, which is in agreement with the experimental observation.[19]

The estimates of γ given in Tables V–VIII were obtained from the free energy values. These computations are expensive since they require a series of molecular simulations. One can also obtain an estimate of γ in a quick and dirty manner by ignoring the contribution of the entropy, i.e., estimate the interfacial excess internal

TABLE VII. Interfacial free energy of various crystallographic planes of orcinol polymorphs (form I and form II) in contact with chloroform. The figure in the parentheses is the uncertainty in the last digit for a confidence interval of 95%.

Polymorphs	Form I				Form II			
Planes	100	010	001	Average	100	010	001	Average
γ (mN/m)	64(1)	71(1)	96(1)	77(1)	64(1)	61(1)	88(1)	71(1)

TABLE VIII. Interfacial free energy of various crystallographic planes of orcinol polymorphs (form I and form II) in contact with nitromethane. The figure in the parentheses is the uncertainty in the last digit for a confidence interval of 95%.

Polymorphs	Form I				Form II			
Planes	100	010	001	Average	100	010	001	Average
γ (mN/m)	59(1)	63(2)	74(1)	65(1)	58(2)	46(2)	63(2)	56(2)

TABLE IX. Comparison of the values of γ and γ' for some crystal planes of each polymorphs of orcinol. The units are in mN/m. The figure in the parentheses is the uncertainty in the last digit for a confidence interval of 95%.

		Chloroform		Nitromethane	
	Planes	Form I	Form II	Form I	Form II
γ	100	64(1)	64(1)	59(1)	58(2)
	010	71(1)	61(1)	63(2)	46(2)
	001	96(1)	88(1)	74(1)	63(2)
γ'	100	46(1)	40(2)	28(2)	21(2)
	010	43(2)	31(1)	34(2)	15(1)
	001	73(1)	88(2)	41(2)	39(2)

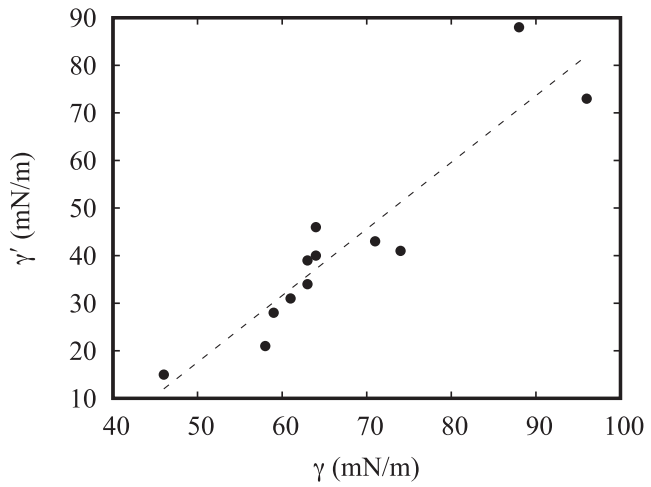

FIG. 8. Comparison of the values of γ and γ' for some crystal planes of each polymorphs of orcinol. The dashed line is a fit of the data and shows the correlation between γ and γ'.

energy, γ', as follows:

$$\gamma' = \frac{U - U^{(s)} - U^{(l)}}{A}, \tag{26}$$

where U is the potential energy for the two phase system and $U^{(s)}$ and $U^{(l)}$ are the potential energies for bulk solid and bulk liquid, respectively. One can then ask whether the values of γ can be reasonably approximated by those for γ'. A comparison of γ and γ' is shown in Table IX and Fig. 8. While there appears to be some correlation between the values of γ and γ', this comparison tells us that there is a significant contribution of entropy to the interfacial free energy, and hence, γ' is a poor estimate of γ.

VII. CONCLUSIONS

In this article, we have presented two direct methods for computing solid–liquid interfacial free energy from molecular simulations via thermodynamic integration. The methods are applicable to systems when (i) the solid phase is sparingly soluble in the liquid and (ii) there is no surface diffusion of molecules in the solid phase. As a representative system, the interfacial free energy was computed for two anhydrous polymorphs of orcinol in contact with solvents, chloroform and nitromethane. The computed values from these two completely independent methods agree with each other, thereby indirectly confirming the accuracy of our estimates. The values of interfacial free energy were also used in combination with the classical nucleation theory to predict the solvent induced polymorph selectivity of orcinol. The predicted polymorph selectivity in nitromethane agrees with the experimental observations but does not for chloroform. An added benefit of our proposed methods is that these simulations can be performed using the publicly available molecular dynamics packages such as LAMMPS,[12] thus obviating the need to write new *à la carte* codes.

SUPPLEMENTARY MATERIAL

See the supplementary material for input files to perform the various simulations described in this paper using the LAMMPS[12] molecular dynamics package.

ACKNOWLEDGMENTS

The computations were carried out using computers purchased under the Nano Mission Programme of Department of Science and Technology, Government of India [Grant No. DST/NM/NS-14/2011(C)] and the Cray Supercomputer of Indian Institute of Science, Bengaluru.

APPENDIX: EXCLUSION OF TRANSLATIONAL DEGREE OF FREEDOM FROM SOLID PHASE PARTITION FUNCTION

In the methods described in this article, free energy contribution arising from the translational degree of freedom of the solid phase was excluded while computing the interfacial free energy. The necessity for this exclusion can be easily explained using the following example. Consider a solid slab exposed to vacuum. Let V be the total volume of this system (slab + vacuum). The Helmholtz free energy of this system, F, can be written as

$$F = F^{(s)} + \gamma A. \tag{A1}$$

While computing the partition function of the solid slab, one can integrate the translational degree of freedom of the slab. Hence, the total partition function can be written as a product of the volume of the system and the partition function of the slab with the translational degree of freedom removed, i.e.,

$$Q(N, V, T) = VQ^*(N, T). \tag{A2}$$

Substituting the above equation into Eq. (A1), we get

$$\begin{aligned}\gamma &= \frac{F - F^{(s)}}{A} \\ &= -k_B T \frac{\ln V + \ln Q^* - \ln Q^{(s)}}{A}.\end{aligned} \tag{A3}$$

From the above expression, γ is dependent on V whose value is totally arbitrary. Hence, the correct and rigorous way to compute γ is to exclude the contribution of the translational degree of freedom of the solid phase from the partition function.

DATA AVAILABILITY

The data that support the findings of this study are available from the corresponding author upon reasonable request.

REFERENCES

[1] D. Bonn, J. Eggers, J. Indekeu, J. Meunier, and E. Rolley, Rev. Mod. Phys. **81**, 739 (2009).
[2] M. Bavière, *Basic Concepts in Enhanced Oil Recovery Processes* (SCI, 1991), Vol. 33.
[3] A. Otten and S. Herminghaus, Langmuir **20**, 2405 (2004).
[4] A. Louhichi, E. Tamborini, N. Ghofraniha, F. Caton, D. Roux, J. Oberdisse, L. Cipelletti, and L. Ramos, Phys. Rev. E **87**, 032306 (2013).

[5]V. D. Nguyen, Z. Hu, and P. Schall, Phys. Rev. E **84**, 011607 (2011).
[6]D. K. Owens and R. C. Wendt, J. Appl. Polym. Sci. **13**, 1741 (1969).
[7]J. Bokeloh, R. Rozas, J. Horbach, and G. Wilde, Phys. Rev. Lett. **107**, 145701 (2011).
[8]J. Q. Broughton and G. H. Gilmer, J. Chem. Phys. **84**, 5759 (1986).
[9]R. L. Davidchack and B. B. Laird, J. Chem. Phys. **118**, 7651 (2003).
[10]R. Benjamin and J. Horbach, J. Chem. Phys. **141**, 044715 (2014).
[11]X. Qi, Y. Zhou, and K. A. Fichthorn, J. Chem. Phys. **145**, 194108 (2016).
[12]S. Plimpton, J. Comput. Phys. **117**, 1 (1995).
[13]J. R. Morris and X. Song, J. Chem. Phys. **119**, 3920 (2003).
[14]F. Leroy, D. J. V. A. dos Santos, and F. Müller-Plathe, Macromol. Rapid Commun. **30**, 864 (2009).
[15]J. R. Espinosa, C. Vega, and E. Sanz, J. Chem. Phys. **141**, 134709 (2014).
[16]E. M. Grzelak and J. R. Errington, J. Chem. Phys. **128**, 014710 (2008).
[17]A. Malani, A. Raghavanpillai, E. B. Wysong, and G. C. Rutledge, Phys. Rev. Lett. **109**, 184501 (2012).
[18]R. K. Reddy A and S. N. Punnathanam, Mol. Simul. **44**, 781 (2018).
[19]A. Mukherjee, P. Grobelny, T. S. Thakur, and G. R. Desiraju, Cryst. Growth Des. **11**, 2637 (2011).
[20]D. M. Huang and D. Chandler, Phys. Rev. E **61**, 1501 (2000).
[21]C. Vega and E. G. Noya, J. Chem. Phys. **127**, 154113 (2007).
[22]J. L. Aragones, E. G. Noya, C. Valeriani, and C. Vega, J. Chem. Phys. **139**, 034104 (2013).
[23]In order to implement the wall interaction using LAMMPS without modifying it, each site for the wall is split into two: one for repulsive and the other for attractive interaction.
[24]W. G. Hoover, Phys. Rev. A **31**, 1695 (1985).
[25]W. L. Jorgensen and T. B. Nguyen, J. Comput. Chem. **14**, 195 (1993).
[26]W. L. Jorgensen, D. S. Maxwell, and J. Tirado-Rives, J. Am. Chem. Soc. **118**, 11225 (1996).
[27]R. W. Hockney and J. W. Eastwood, *Computer Simulation Using Particles* (CRC Press, 1988).
[28]G. Bussi and M. Parrinello, Phys. Rev. E **75**, 056707 (2007).